Theoretical and experimental study of feed network effects on the radiation pattern of series-fed microstrip antenna arrays

K.-L. Wu
M. Spenuk
J. Litva
D.-G. Fang

Indexing terms: Antennas, Radiation

Abstract: Microstrip series-fed arrays are often utilised for compact array designs. This type of feed structure minimises feedline lengths and feedline radiation. However, in practice, the radiation from the feed network still can be significant and it can have a noticeable effect on the array radiation pattern. Analysis is performed using the advantageous full-wave discrete image technique. Theoretical and experimental analysis of the radiation from a four-element series-fed microstrip array antenna, which fully includes the effect of the feed network, is presented. General conclusions are made for the purpose of practical designs.

1 Introduction

In this paper, the full-wave discrete-image technique is used to analyse a microstrip antenna array. Specifically, it is used to study the effect of the feed network on a series-fed microstrip antenna array. The image technique allows an entire array, including its feed network, to be treated as an irregularly shaped patch antenna, which can then be analysed by means of the moment method.

A recent advance in the analysis of microstrip antennas has been the application of integral equation techniques, using the Sommerfeld-type Green function. The numerical integral techniques have been used to analyse individual elements, as well as mutual coupling between the elements in an array. Consequently, many algorithms have been developed for calculating efficiently the inverse transform of the Sommerfeld type Green function. The full-wave discrete-image technique [1] is one of the suit of recently developed algorithms. The advantage of the technique is that it turns a spectral domain problem into a spatial domain problem without losing any full-wave information. Therefore it is very suitable for applications to microstrip antennas with large dimensions, such as arrays.

A microstrip series-fed array [2] consists of a linear array of microstrip patch antennas connected in series by a microstrip transmission line. This type of feed structure tends to minimise the feedline lengths and thereby minimises the radiation from the feed network. In practice, it is found that the radiation from the feed network still has a significant magnitude and can therefore have a noticeable effect on the array radiation pattern.

In the past few years, some work has been done on the feed-network effects of microstrip antenna arrays [3, 4]. One of these studies has focused only on the calculation of the array input impedance using a semifull wave model. In this model, the feed network was treated as an ideal transmission line that was decoupled from the patch elements. Unfortunately, this assumption is not valid for most applications. On the other hand, the transmission line radiation effects have been taken into account, based only on the assumption of a pure travelling current wave on the feed network. Because of the limitations of the early work, it is difficult to draw any general conclusions regarding the contribution of the feed network to the radiation pattern. Therefore it is of interest to carry out a general analysis of the feed network effects on the radiation pattern of an array.

The primary objective of this paper is to present an analysis of the radiation from a microstrip array antenna, that fully includes the effect of the feed network. In particular, the array feed network is analysed with a standing current wave, using an efficient and accurate full-wave discrete-image technique. The condition where a standing current wave exists on the feed network is the most general form of the problem. Normally, the impedance of elements of an array are matched to the feed structure to prevent standing waves. In the case of series-fed arrays, though, there is usually uncertainty associated with the derivation of the impedance of the elements due to mutual coupling. This leads to an uncertainty with regard to the matching condition, which in turn results in at least parts of the array feed network having standing waves. The results from the analysis that is carried out here, using standing waves, can be used by the antenna designer to take into account the effects of radiation from the feed network. The fact that the image technique used for the analysis is applied only to series-fed arrays in this paper should not suggest that the technique does not have broad applications. In fact, its potential applications are quite broad. This paper will present general conclusions with regard to the radiation from standing waves on the feed network of a series-fed array. These results will serve as a guide to the reader when designing practical array antennas.

Paper 7957H (E11), first received 20th April and in revised form 31st August 1990

K.-L. Wu, M. Spenuk and J. Litva are with the Communications Research Laboratory, McMaster University, Ontario, Canada L85 4K1

D.G. Fang is with the Department of Electrical Engineering, East China Institute of Technology, Nanjing, People's Republic of China

2 Radiation loss from microstrip lines

Consider a segment of planar microstrip line with an arbitrary load on one end and matched source on the other end. The current on the transmission line which is fed by the source current $I_0 e^{j\omega t}$ can be expressed as

$$\boldsymbol{J}(y) = I_0(e^{-j\beta y} - \Gamma e^{j\beta y})/W_e\hat{\boldsymbol{y}} \tag{1}$$

where Γ = the reflection coefficient at the load end of the line, W_e = the width of the line, and β = the constant of propagation in the transmission line.

The real part of the complex input power is dissipated by two mechanisms. One is by radiation loss into space, which occurs within the 'visible range' given by $k_x^2 + k_y^2 < k_0^2$. Another is by propagation of surface waves, which occurs in the 'invisible range'. The surface wave region is defined by the condition $k_x^2 + k_y^2 > k_0^2$. For small d/λ, the fraction of the total input power that is converted into surface waves varies as $(d/\lambda)^3$, whereas that radiated into free space varies as $(d/\lambda)^2$ [5, 6]. Therefore under these conditions, the portion of the power radiated into space is considerably larger than that converted into surface waves. As well, the power converted into surface waves does not affect the characteristics of that radiated into space under the assumption of infinitely large substrate. Based on these two considerations, we focus on the space-radiated power, that is, the real part of the complex power that appears in the visible range, as defined above.

The power radiated into free space is given by [7]

$$P_r^{total} = \int_0^{\pi/2}\int_0^{2\pi} f(\theta, \phi)\sin\theta\, d\theta\, d\phi \tag{2}$$

where

$$f(\theta, \phi) = \frac{15k_0^2}{\pi}\left(\frac{|-\tilde{J}_x\sin\phi + \tilde{J}_y\cos\phi|^2\cos^2\theta}{(\varepsilon_r - \sin^2\theta)\cot^2[dk_0\sqrt{(\varepsilon_r - \sin^2\theta)}] + \cos^2\theta} + \frac{|\tilde{J}_x\cos\phi + \tilde{J}_y\sin\phi|^2\cos^2\theta(\varepsilon_r - \sin^2\theta)}{(\varepsilon_r - \sin^2\theta) + \varepsilon_r^2\cos^2\theta\cot^2[dk_0\sqrt{(\varepsilon_r - \sin^2\theta)}]}\right) \tag{3}$$

is the radiation power pattern that can be derived directly from the far field pattern discussed in Reference 5. $\tilde{J}_x$ and $\tilde{J}_y$ are the Fourier transforms of the x and y components of the current.

For purposes of comparison, E-plane radiation loss and H-plane radiation loss are defined to be proportional to the radiation lost in each of these planes, that is

$$P_r^E = 2\pi\int_{-\pi/2}^{\pi/2} f\left(\theta, \frac{\pi}{2}\right)d\theta \tag{4}$$

$$P_r^H = 2\pi\int_{-\pi/2}^{\pi/2} f(\theta, 0)\, d\theta \tag{5}$$

To calculate the radiation losses from the current on a transmission line, the Fourier transform of the current eqn. 1 is needed, which is

$$\tilde{J}_y(k_x, k_y) = I_0\left\{\frac{e^{j(k_y-\beta)L} - 1.0}{j(k_y - \beta)} - \Gamma\frac{e^{j(k_y+\beta)L} - 1.0}{j(k_y + \beta)}\right\} \times \frac{\sin\left(\frac{k_x W_e}{2}\right)}{\frac{k_x W_e}{2}} \tag{6}$$

where

$$k_x = k_0\sin\theta\cos\phi \quad k_y = k_0\sin\theta\sin\phi \tag{7}$$

and L is the length of the line.

If eqn. 6 is substituted into eqn. 3, then eqn. 3 into eqns. 2, 4 and 5, a set of representative results is obtained. Total radiation loss, E-plane radiation loss and H-plane radiation loss versus line length are given in Fig. 1. It is

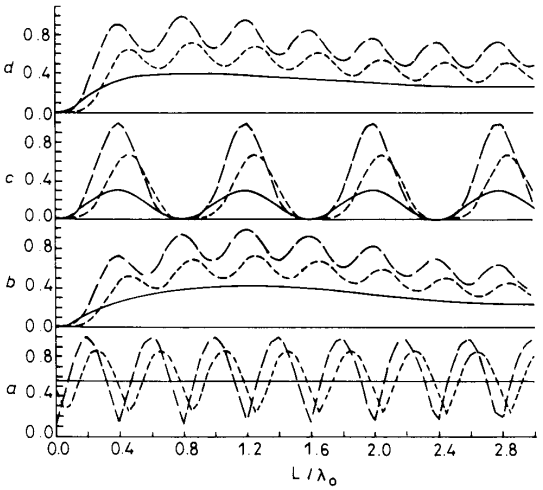

Fig. 1 *Normalised radiation lost against the current distribution on a microstrip line*

——— $\Gamma = (0, 0)$
– – – – $\Gamma = (0.8, 0)$
------- $\Gamma = (0.3, -0.5)$
$\varepsilon_r = 2.1$; $h = 1.5748$ mm; $W = 1.3$ mm; $f = 9.42$ GHz
a current distribution on the microstrip line
b E-plane radiation loss
c H-plane radiation loss
d total radiation loss

assumed that there is a standing wave condition on the microstrip line. The parameters for the line are: dielectric constant $\varepsilon_r = 2.1$, substrate thickness $d = 1.5748$ mm, and feed line width $W = 1.3$ mm. The general conclusions concerning the end-fed line with standing current can be drawn as follows:

(*a*) for a given feedline, the radiation losses vary with the magnitude of the reflection coefficient Γ at the load end of the line. The greater the amplitude of Γ, the higher the average radiation loss. When Γ equals (0.0, 0.0), the level of the radiation loss is at a minimum. In general, to minimise the radiation loss a good matching condition is desired.

(*b*) when Γ does not equal (0.0, 0.0), the radiation loss varies with the characteristics of the current standing wave pattern. The values of the radiation loss parameters for P_r^{total} and P_r^E assume local minima at current nulls and local maxima at current peaks. The H-plane radiation loss parameter, on the other hand, goes to zero for line lengths with an even number of standing waves and assumes a maxima for an odd number of standing waves. These facts suggest that there is an optimum line length for reducing losses from the feed network.

(*c*) for a given feed network, the radiation loss increases rapidly in the range $0 < L < 0.4\lambda_0$, and the ripple on the patterns in Fig. 1 does not change significantly with increase in line length. Radiation loss in the H-plane is much less than that in the E-plane, due to there being no x-directed current.

In general, the feed network is not a simple structure, consisting only of transmission line, but rather it may also consist of matching networks, as well as filters. It follows that, in a practical design, the current distribution on the feed network needs to be derived along with the current distribution on the array. This task can be accomplished by using the full-wave technique described in the next section.

3 Full-wave discrete image technique and moment method solution

For simplicity, the discussion here is restricted to the single-layer microstrip case. If one considers an x-directed horizontal electric dipole embedded in the substrate, the x-component of the space domain vector potential can be written as

$$A_G^{xx} = \frac{1}{4\pi}\int_0^\infty \frac{\mu}{j2k_z}\{T_{TE}^{\pm}\}J_0(k_\rho\rho)k_\rho\,dk_\rho \tag{8}$$

and the scalar potential can be written as

$$\Phi_G = \frac{1}{4\pi}\int_0^\infty \frac{1}{j\omega\varepsilon}\frac{1}{j2k_z}\left\{T_{TE}^{\pm} + \frac{k_z^2}{k_\rho^2}\left(T_{TE}^{\pm} \pm \frac{1}{jk_z}\frac{\partial T_{TM}^{\pm}}{\partial z}\right)\right\} \times J_0(k_\rho\rho)k_\rho\,dk_\rho \tag{9}$$

where ε, μ and k_z denote the source region permittivity, permeability and the z-component of the wavenumber, respectively. $T_{TE}^{\pm}$ and $T_{TM}^{\pm}$ denote the spectral domain transmisssion coefficients of TE and TM waves, respectively. A detailed description of these components is given by Reference 1.

Owing to the complexity of Sommerfeld-type integrals given by eqns. 8 and 9, it is impractical to analyse a microstrip antenna array using conventional numerical integration procedures [8]. The full-wave discrete-image technique provides a powerful tool for carrying out this task. The idea underlying the technique is the use of the Prony method to approximate the spectral domain Green function (the terms inside the braces in eqns. 8 and 9), by a series of complex exponential functions. As an initial guess, one may start with

$$\tilde{A}_G^{xx} = \{T_{TE}^{\pm}\} = \sum_{i=1}^{N_i} a_i e^{b_i k_z} \tag{10}$$

and then carry out a search for the best approximation using an optimisation procedure, based on the objective function

$$F = \int_{L_p} W(k_\rho)\left|\tilde{A}_G^{xx}(k_\rho) - \sum_{i=1}^{N_i} a_i e^{b_i k_z(k_\rho)}\right|^2 dl \tag{11}$$

where N_i = the number of images, generally less than 5; a_i and b_i are complex coefficients; and k_ρ is the wave number in the horizontal direction. The integration path L_p is the same as that used in the Prony method which is fully discussed in Reference 1. The choice of the weighting function $W(k_\rho)$ is based on the behaviour of the approximated function.

Once the complex parameters a_i and b_i are determined for a given substrate, the inverse Fourier transforms of eqns. 8 and 9 can be easily carried out analytically by using the Sommerfeld identity. That is to say, the complicated Green functions defined by eqns. 8 and 9 become simple Green functions in free space. The advantage of using this technique will become obvious when we discuss the moment procedure next.

With reference to Fig. 2, the boundary condition for the electric field on the surface of the array is

$$\hat{z} \times (\boldsymbol{E}^s(\boldsymbol{r}) + \boldsymbol{E}^e(\boldsymbol{r})) = 0 \tag{12}$$

where the scattering field $\boldsymbol{E}^s$ can be defined using the vector potential $\boldsymbol{A}$ and the scalar potential Φ as

$$\boldsymbol{E}^s(\boldsymbol{r}) = -j\omega\boldsymbol{A} - \nabla\Phi \tag{13}$$

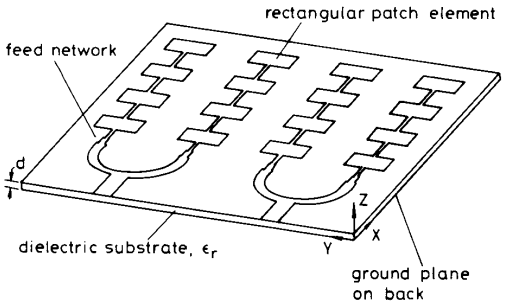

Fig. 2 *Series-fed microstrip antenna array*

and impressed field $\boldsymbol{E}^e$ is assumed to be a δ generator at the input of the feed network. These potentials are expressed in terms of the corresponding dyadic Green function $\vec{A}_G$ and Φ_G. One element of $\vec{A}_G$, that is A_G^{xx} was defined previously by eqn. 8, and Φ_G has been defined by eqn. 9. The potentials in eqn. 13 can be defined in terms of integrals of the charge and current densities q_s and $\boldsymbol{J}_s$ as

$$\Phi(\rho) = \iint_s \Phi_G(\rho\,|\,\rho')q_s(\rho')\,dS' \tag{14}$$

$$\boldsymbol{A}(\rho) = \iint_s \vec{A}_G(\rho\,|\,\rho')\boldsymbol{J}_s(\rho')\,dS' \tag{15}$$

Finally, eqn. 12 can be rewritten in integral equation form as

$$\hat{z} \times \boldsymbol{E}^e(\rho) = \hat{z} \times \left[j\omega \iint_s \vec{A}_G(\rho\,|\,\rho')\boldsymbol{J}_s(\rho')\,dS' + \nabla \iint_s \Phi_G(\rho\,|\,\rho')q_s(\rho')\,dS'\right] \tag{16}$$

To solve eqn. 16 for an irregularly shaped microstrip antenna, the moment procedure using rooftop basis functions and line matching test functions, as shown in Fig. 3,

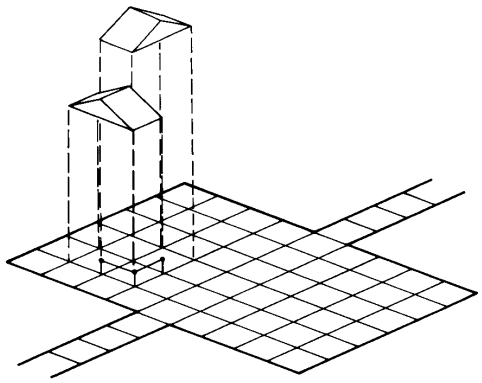

Fig. 3 *Rooftop elements and integration paths*

is selected in this study. This approach was successfully used by Reference 9 in a study of a single microstrip antenna. In this model, every current cell supports one rooftop basis, and two charge cells correspond to each of the current cells. The current cells half overlap each other, and one test segment is located at the centre of each current cell. Therefore the surface current is expanded as

$$J_{sx} = \frac{1}{b}\sum_{i=1}^{M} I_{xj}\, T_X(\boldsymbol{r} - \boldsymbol{r}_{xj}) \tag{17a}$$

$$J_{sy} = \frac{1}{a}\sum_{i=1}^{N} I_{yj}\, T_Y(\boldsymbol{r} - \boldsymbol{r}_{yj}) \tag{17b}$$

where $\boldsymbol{r}_{xj}$ and $\boldsymbol{r}_{yj}$ is the centre vector of x-directed and y-directed current elements respectively, and

$$T_X(\boldsymbol{r}) = \begin{cases} 1 - |x|/a & |x| < a \quad |y| < b/2 \\ 0 & \text{elsewhere} \end{cases} \tag{17c}$$

A similar expression for T_Y can be obtained by interchanging $a \leftrightarrow b$ and $X \leftrightarrow Y$. By use of the continuity equation and the expressions in eqn. 17, the charge density is obtained:

$$q_x = \frac{1}{j\omega ab}\left\{\sum_{j=1}^{m} I_{xj}[\Pi(\boldsymbol{r} - \boldsymbol{r}_{xj}^{+}) - \Pi(\boldsymbol{r} - \boldsymbol{r}_{xj}^{-})] + \sum_{j=1}^{m} I_{yj}[\Pi(\boldsymbol{r} - \boldsymbol{r}_{yj}^{+}) - \Pi(\boldsymbol{r} - \boldsymbol{r}_{yj}^{-})]\right\} \tag{18}$$

Inserting both eqns. 17 and 18 into eqn. 16, then applying the testing procedure by integrating the boundary condition along the segments linking the centres of adjacent charge cells, one obtains the following equations:

$$j\omega \int_{cx_i} A_x\, dx + \Phi(\boldsymbol{r}_{\xi}^{+}) - \Phi(\boldsymbol{r}_{\xi}^{-}) = \int_{cx_i} E_x^e\, dx \tag{19a}$$

$$j\omega \int_{cy_i} A_y\, dy + \Phi(\boldsymbol{r}_{yi}^{+}) - \Phi(\boldsymbol{r}_{yi}^{-}) = \int_{cy_i} E_y^e\, dy \tag{19b}$$

where

$$A_x = \frac{1}{b}\sum_{j=1}^{M} I_{xj} \iint_{S_{xj}} A_G^{xx} T_X(\boldsymbol{r}' - \boldsymbol{r}_{xj})\, dS' \tag{20a}$$

$$A_y = \frac{1}{a}\sum_{j=1}^{N} I_{yj} \iint_{S_{yj}} A_G^{yy} T_Y(\boldsymbol{r}' - \boldsymbol{r}_{yj})\, dS' \tag{20b}$$

$$\Phi(\boldsymbol{r}) = \frac{1}{jab\omega}\left\{\sum_{j=1}^{M} I_{xj}\left[\iint_{S_{oj}} \Phi_G(\boldsymbol{r}\,|\,\boldsymbol{r}')\Pi(\boldsymbol{r}' - \boldsymbol{r}_{xj}^{+})\, dS' - \iint_{S_{oj}} \Phi_G(\boldsymbol{r}\,|\,\boldsymbol{r}')\Pi(\boldsymbol{r}' - \boldsymbol{r}_{xj}^{-})\, dS'\right] + \sum_{j=1}^{N} I_{yj}\left[\iint_{S_{oj}} \Phi_G(\boldsymbol{r}\,|\,\boldsymbol{r}')\Pi(\boldsymbol{r}' - \boldsymbol{r}_{yj}^{+})\, dS' - \iint_{S_{oj}} \Phi_G(\boldsymbol{r}\,|\,\boldsymbol{r})\Pi(\boldsymbol{r}' - \boldsymbol{r}_{yj}^{-})\, dS'\right]\right\} \tag{20c}$$

The current coefficient I_{xj} and I_{yj} can be obtained after solving eqn. 19, provided that the excitation field $\boldsymbol{E}^e$ is given. It is worth mentioning that only the free-space Green functions are involved in the computation of eqn. 19. The moment procedure can be considered as a conventional moment procedure in free space. This feature is obviously important when a microstrip antenna array needs to be analysed. From the current distribution obtained by the moment soluton, we can find the radiation patterns, as well as all the other parameters of interest with regard to the antenna's characteristics.

4 Numerical and experimental results

With the objective of investigating the effect of the feed network on a practical series-fed microstrip antenna array, a four-element array is studied both numerically and experimentally. The layout is shown in Fig. 4*b*. For

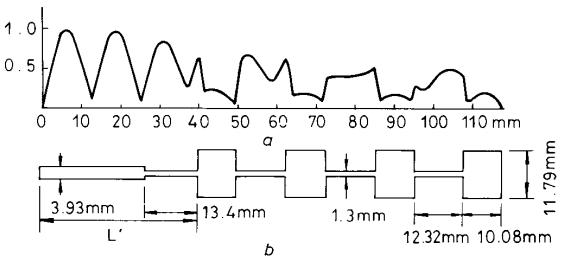

Fig. 4 *Four-element array*
a current distribution on the array and feed line at working frequency 9.42 GHz
b series-fed subarray and physical dimensions

simplicity, the feed network only includes a simple step discontinuity.

The whole array system is divided into rectangular element cells, on which the moment procedure is applied. A two-dimensional distributed current is then determined, once the excitation is given. In this example, a δ-gap excitation source located near the end of the feed network is used. In Fig. 4*a*, the current distribution along the centre line of the array is shown. Based on the current distribution, the effects of the feed network on the radiation pattern can be predicted in a straightforward manner.

Because of impedance mismatches, a standing current wave exists on the feed network. According to the conclusions in Section 2, the effect of the feed network will vary with its length. Figs. 5–7 show the E-plane radiation patterns for the array with different lengths of feed network. When the feed network includes only one-half of a standing wave current, as shown in Fig. 5 (with $L' = 15$ mm), the radiation pattern is degraded. It has higher sidelobe levels and a wider mainlobe, as compared to the case where the feed line effects are not present, as shown in Fig. 8. If the length L' is now adjusted, such that it includes more and more of the next standing wave, we can find a length (in this case $L' = 28$ mm), where the

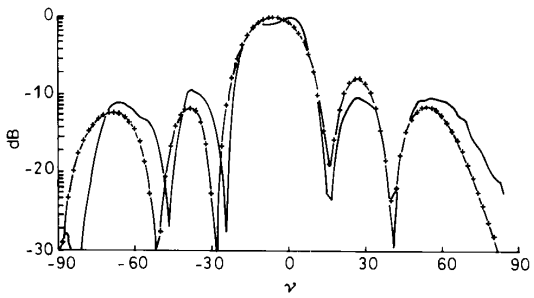

Fig. 5 *E-Plane radiation patterns with $L' = 15$ mm*
——— measured
+++ theory

effects are greatly diminished and there is a corresponding improvement in the pattern. This condition is shown in Fig. 6 and comes about because of cancellation between opposing currents. It should be noted that due to the nonuniformity of the feed network and the

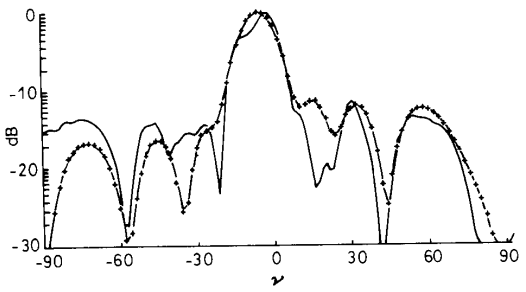

Fig. 6 *E-Plane radiation patterns with L = 28 mm*
——— measured
+ + + theory

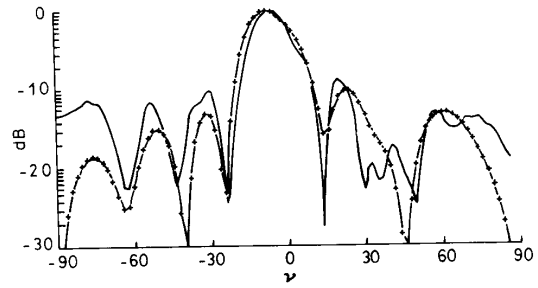

Fig. 7 *E-Plane radiation patterns with L = 37 mm*
——— measured
+ + + theory

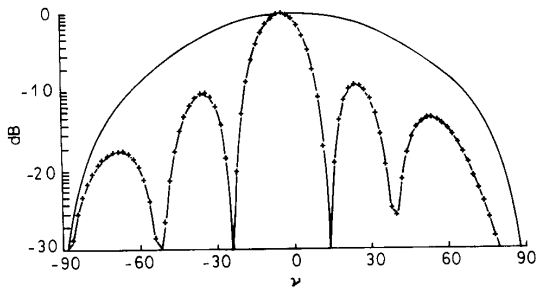

Fig. 8 *Theoretical radiation patterns of the array without feed network*
+ + + *E*-plane pattern
——— *H*-plane pattern

resulting nonuniform current distribution, the pattern which is least distorted by the feedline is not the one which corresponds to a peak occurring in the standing wave pattern. When we increase the length still further, to include the third standing wave, the pattern degrades once again. This is shown in Fig. 7 with $L = 37$ mm. In Figs. 4–6, the theoretical results are compared with experimental results, and the agreement is seen to be very good.

Because an infinitely large substrate is assumed in the theoretical model, scattering of surface waves from the edges of a finite substrate is not taken into account in our analysis. The significance of such scattering, which occurs at $\theta = \pm 90°$, can be seen in the discrepancy between the predicated and measured patterns at $\theta = \pm 90°$, in Figs. 5–7.

5 Conclusions

A full-wave theoretical approach is presented for carrying out analysis of microstrip arrays, which includes the effect of the feed network. Since no impractical assumptions are used in the array model, and a highly efficient numerical technique is used to calculate the Sommerfeld-type integral, it is expected that the technique used in this paper will find a wide range of applications in microstrip array design.

General conclusions were presented with regard to the effect of the feed network on the radiation patterns of the array antenna. These can be used as a guideline for practical designs. Since the radiation from feed networks varies with their dimensions and current distributions, these parameters can be adjusted by designers so as to minimise the degradation in the antenna pattern. To show the applicability and validity of the full-wave discrete-image technique to microstrip arrays, a practical four-element series-fed array has been studied both theoretically and experimentally. The experimental results show very close agreement with the theoretical results.

Although only the *E*-plane radiation patterns were studied, the results can be used for deriving other parameters such as input impedance. The modelling for a large array using an entire domain basis function is currently under development.

6 Acknowledgments

The authors gratefully acknowledge financial support by the Natural Science and Engineering Research Council of Canada (NSERC) and Telecommunication Research Institute of Ontario (TRIO). The authors would like to thank Mr. Jian Wang for many helpful discussions. The suggestions made by the reviewers of the paper are also acknowledged.

7 References

1 FANG, D.G., YANG, J.J., and DELISLE, G.Y.: 'Discrete image theory for horizontal electric dipoles in a multilayered medium', *IEE Proc. H, Microwaves, Antenna & Propagat.*, 1988, **135**, pp. 297–303
2 METZLER, T.: 'Microstrip series arrays', *IEEE Trans.*, 1981, **AP-29**, pp. 174–178
3 NEWMAN, E.H., and TECHAN, J.E.: 'Analysis of a microstrip array and feed network', *IEEE Trans.*, 1985, **AP-33**, pp. 397–403
4 LEVINE, E., MALAMUD, G., SHTRIKMAN, S., and TREVES, D.: 'A study of microstrip array antennas with the feed network', *IEEE Trans.*, 1989, **AP-37**, pp. 426–434
5 PERLMUTTER, P., SHTRIKMAN, S., and TREVES, D.: 'Electric surface current model for the analysis of microstrip antennas with application to rectangular elements', *IEEE Trans.*, 1985, **AP-33**, pp. 301–311
6 CHANG, D.C.: 'Analytical theory of an unloaded rectangular microstrip patch', *IEEE Trans.*, 1981, **AP-29**, pp. 54–62
7 UZUNOGLU, N.K., ALEXOPOULOS, N.G., and FIKIORIS, J.G.: 'Radiation properties of microstrip dipoles', *IEEE Trans.*, 1979, **AP-27**, pp. 853–858
8 POZAR, D.M.: 'Input impedance and mutual coupling of rectangular microstrip antennas', *IEEE Trans.*, 1982, **AP-30**, pp. 1191–1196
9 MOSIG, J.R., and GARDIOL, F.E.: 'General integral equation formulation for microstrip antennas and scatterers', *IEE Proc. H, Microwaves, Antenna & Propagat.*, 1985, **132**, pp. 424–432